Transient EHL Analysis on Spur Gear Teeth with Consideration of Gear Kinematics

Young-Pil Koo*

School of Mechanical Engineering, Pukyong National University, Busan, 608-739, Korea

Transient 3-dimensional elasto-hydrodynamic lubrication (EHL) analysis is performed on the contacting teeth surfaces of involute spur gears. Kinematics of the gear and the pinion are taken into account to get accurate geometric clearance around the EHL region of the contacting teeth. The surface pressure and film thickness distribution for the whole contact faces in a lubricated condition at several time steps are obtained through the analysis. Besides the pressure spike at the outlet region, a representative phenomenon in EHL regime, the pressure at the inlet region is slightly higher than that of the center region. The film thickness of transient condition is thicker than that of steady condition.

Key Words : Elasto-Hydrodynamic Lubrication, Spur Gear, Kinematics, Transient

Nomenclature

a : Pressure-viscosity coefficient [m^2/N]
E : Effective modulus of elasticity [N/m^2]
G : Dimensionless material parameter, $G=aE$
H : Dimensionless film thickness
h : Film thickness [m]
P : Dimensionless EHL pressure
p : EHL pressure [N/m^2]
R : Equivalent radius [m]
R_i : Radius of curvature of gear or pinion tooth [m] ($i=1$ for gear, $i=2$ for pinion)
R_{bi} : Base circle radius of gear or pinion [m]
R_{ai} : Addendum circle radius of the gear or pinion [m]
R_{pi} : Pitch circle radius of the gear or pinion [m]
r_i : Radius in polar coordinates [m]
T : Dimensionless time
t : Time [s]
U : Dimensionless velocity parameter
$\tilde{u}$: Mean surface velocity [m/s]
u_i : Surface velocity of the gear or pinion tooth [m/s]
w : External load [N]
X, Y : Dimensionless Cartesian coordinates
x, y : Global Cartesian coordinates
x_i, y_i : Local Cartesian coordinates
Z : Dimensionless viscosity-pressure index
α : Pressure angle [rad]
η : Absolute viscosity [Ns/m^2]
η_0 : Absolute viscosity at $p=0$ [Ns/m^2]
$\bar{\eta}$: Dimensionless absolute viscosity
θ_i : Rotation angle of the gear or pinion [rad]
ρ : Density [Ns^2/m^4]
ρ_0 : Density at $p=0$ [Ns^2/m^4]
$\bar{\rho}$: Dimensionless density
ω_1 : Angular velocity of the gear [rad/s]

* **E-mail** : ypkoo@naver.com
TEL : +82-51-620-1621; **FAX** : +82-51-620-1405
School of Mechanical Engineering, Pukyong National University, Busan, 608-739, Korea. (Manuscript **Received** August 19, 2003; **Revised** may 27, 2004)

1. Introduction

Gears are essential elements to transfer power and are widely applied to most machinery. Many studies have been made in the field of design, manufacturing, and test of gears (Seol et al, 2000 and Lee, 1999). As for the study on the surface of contacting gear teeth, Jiang (1999) formed reaction film by using anti-scuffing additives on the gear tooth and studied failure model of the reac-

tion film. Murakawa et al. (1999) coated amorphous carbon thin film on gear tooth face and tested lubricating ability in the case of no lubricant supply. Lyu et al. (1998) studied effects of several surface treatments such as shot peening, chemical polishing and electro-polishing on the bending fatigue strength of the caburized gear teeth. Wu et al. (1993) investigated sliding wear of spur gears.

As gears are typical elements that are working in elasto-hydrodynamic lubrication (EHL) regime (Dowson, 1995), a study on lubrication phenomenon of gear teeth can be much helpful in improving gear design. Larsson (1997) simulated film thickness and pressures along tooth profile with consideration of transient effect and non-Newtonian fluid model. Contact model was 2-dimensional line contact with assumption that gears contacting face was two cylinders contact. Dowson and Higginson (1966) suggested a formula of minimum film thickness between gear teeth with the use of their study in EHL.

The conventional model of clearance shape between gear teeth for the EHL analysis has been approximated to the contact of two cylinders whose radii are set to the radius of curvature at the contact point. But the actual curvature of gear teeth is continuously changing around the contact point, therefore the cylinder contact model cannot describe actual clearance shape of the gear teeth.

In this study, to estimate the lubrication phenomenon on gear teeth contact accurately, procedure to calculate initial clearances between contacting spur gear teeth with consideration of gear kinematics is suggested. EHL pressure distribution and film thickness between gear teeth are obtained by a transient 3-dimensional EHL analysis with the application of the calculated initial clearances.

2. Geometric Clearances Between Gear Teeth

Figure 1 shows contacting spur gear teeth and coordinates systems. The clearances between the gear tooth and the pinion tooth should be known prior to the EHL analysis. Because the contact

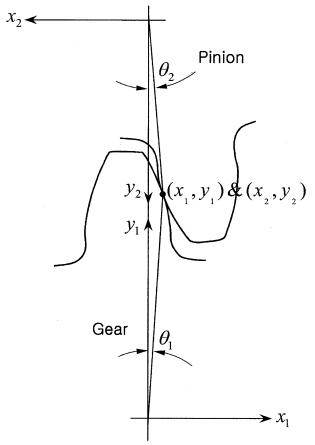

Fig. 1 Schematics of teeth and coordinate systems

points of the teeth move and the contact radii of curvature change as gear rotates, the teeth clearances also change over time. By the following procedure, an accurate geometric clearance shape for a specific time step can be obtained.

a. Tooth profiles of the gear and the pinion are generated by Eq. (1) in local Cartesian coordinates whose origins are located at the center of the gear and the pinion respectively.

$$\begin{aligned} x_i &= R_{bi}(\theta_i \cos\theta_i - \sin\theta_i) \\ y_i &= R_{bi}(\cos\theta_i + \theta_i \sin\theta_i) \end{aligned} \tag{1}$$

The subscrip i equals 1 for gear, 2 for pinion.

b. To find the posture of the gear profile and pinion profile at the starting contact point, the gear profile is rotated so that its outermost point meets the intersection of the gear's outside diameter and the line of action as shown in Fig. 2.

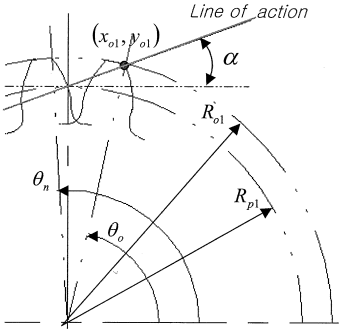

Fig. 2 Setting the initial reference point

Cartesian coordinates of the intersection point are:

$$x_{o1}=\frac{-2R_{p1}\tan\alpha+\sqrt{4R_{p1}^2\tan^2\alpha-4(1+\tan^2\alpha)(R_{p1}^2-R_{o1}^2)}}{2(1+\tan^2\alpha)}$$
$$y_{o1}=x_{o1}\tan\alpha+R_{p1} \quad (2)$$

Then, pinion profile is rotated until the initial contact point on the pinion profile matches the above intersection point. As shown in Eq. (3), the initial contact point on the pinion profile is the one from which the distance to the origin of the pinion is the same as the distance from the intersection point to the origin.

$$\sqrt{x_2^2+y_2^2}=\sqrt{(-x_{o1})^2+(R_{p1}+R_{p2}-y_{o1})^2} \quad (3)$$

c. To get the moved profile posture by the successive rotation of gear and pinion, the local Cartesian coordinates are converted to the local polar coordinates making use of Eq. (4).

$$r_i=\sqrt{x_i^2+y_i^2}$$
$$\theta_i=\pi/2+\tan^{-1}(-x_i/y_i) \quad \forall\ x_i\le 0,\ y_i>0 \quad (4)$$
$$\theta_i=\tan^{-1}(y_i/x_i) \quad \forall\ x_i>0,\ y_i>0$$

Several rotation angles are selected along the line of action and the gear and the pinion are rotated stepwise to each other. After each step rotation, the local polar coordinates are converted to the global Cartesian coordinates and the profile data are reserved. Figure 3 shows the configuration of both profiles at the step near the pitch point.

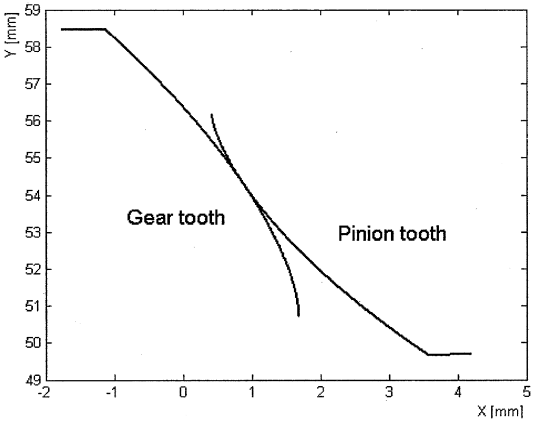

Fig. 3 Configuration of contacting teeth

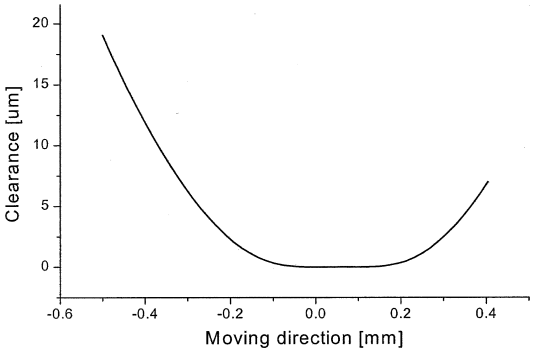

Fig. 4 Initial clearance between the contacting gear teeth

d. To find a contact point of two profiles at each step, the distances between two profiles are calculated. Points in pair whose distance is minimum become contact points numerically.

e. Region for lubrication analysis is set: The inlet region for both the pinion tooth profile and gear tooth profile is the same size, using the contact center as a reference point, In the same way, the outlet region for both profiles is taken. Because the grid sizes of the profiles are not even due to the conversion of a polar to a Cartesian coordinate system, the nodes should be rearranged so as to have an even grid size along the original profiles.

f. Finally, the initial clearances are obtained by calculating distances between two mating nodes:

$$h_g=\sqrt{(x_2-x_1)^2+(y_2-y_1)^2} \quad (5)$$

Figure 4 is the shape of the geometric clearance between two profiles for Fig. 3.

3. EHL Analysis

3.1 Governing equations

The "Reynolds Equation" is adopted to find pressure distributions through transient 3-dimensional EHL analysis (Hamrock, 1994):

$$\frac{\partial}{\partial x}\left(\frac{\rho h^3}{\eta}\frac{\partial p}{\partial x}\right)+\frac{\partial}{\partial y}\left(\frac{\rho h^3}{\eta}\frac{\partial p}{\partial y}\right)=12\tilde{u}\frac{\partial(\rho h)}{\partial x}+12\frac{\partial(\rho h)}{\partial t} \quad (6)$$

The second term on the right hand side of Eq. (6) is the transient term for variation of density and

film thickness with the elapse of time. The dominant effect of the transient term comes from film thickness changes caused by movement of the contact point. The entraining velocity is calculated by Eq. (7).

$$\begin{aligned}\tilde{u}&=(u_1+u_2)/2\\ u_1&=\omega_1(R_{p1}\sin\alpha+x)\\ u_2&=\omega_2(R_{p2}\sin\alpha-x)\end{aligned} \tag{7}$$

The pressure distribution should satisfy the force equilibrium condition in Eq. (8). The resultant force composed by pressures should be balanced to the external load:

$$w=\iint p\,dx\,dy \tag{8}$$

At an EHL regime, dependency of viscosity and density on pressure should be considered (Dowson, 1966 and Roelands, 1966).

$$\eta=\eta_0\left(\frac{\eta_\infty}{\eta_0}\right)^{1-(1+p/C_p)^z} \tag{9}$$

where, $\eta_\infty=6.31\times10^{-5}$ Ns/m^2, $C_p=1.96\times10^8$N/m^2

$$\rho=\rho_0\left(1+\frac{0.6\times10^{-9}p}{1+1.7\times10^{-9}p}\right) \tag{10}$$

3.2 Finite difference formulation

Dimensionless parameters are:

$$X=\frac{x}{R},\ Y=\frac{y}{R},\ H=\frac{h}{R},\ \bar{\eta}=\frac{\eta}{\eta_0},\ \bar{\rho}=\frac{\rho}{\rho_0},$$
$$P=\frac{p}{E},\ U=\frac{\eta_0\tilde{u}}{ER},\ T=\frac{\omega_1 t}{2\pi},\ V=\frac{\omega_1\eta_0}{\pi E}$$

By making use of the dimensionless parameters, Eq. (6) is expressed in dimensionless form:

$$\frac{\partial}{\partial X}\left(\frac{\bar{\rho}H^3}{\bar{\eta}}\frac{\partial P}{\partial X}\right)+\frac{\partial}{\partial Y}\left(\frac{\bar{\rho}H^3}{\bar{\eta}}\frac{\partial P}{\partial Y}\right)=12U\frac{\partial(\bar{\rho}H)}{\partial X}+6V\frac{\partial(\bar{\rho}H)}{\partial T} \tag{11}$$

The effective radius of the first time step in Eq. (12) is adopted as the reference length for the dimensionless film thickness of the whole time steps:

$$R=(1/R_1+1/R_2)^{-1} \tag{12}$$

Equation (13) expresses finite difference approximation by adopting central differences for space and backward differences for time.

$$\begin{aligned}f_{i,j}=&\frac{1}{2}\left\{\left(\frac{\bar{\rho}H^3}{\bar{\eta}}\right)_{i+1,j}+\left(\frac{\bar{\rho}H^3}{\bar{\eta}}\right)_{i,j}\right\}\frac{P_{i+1,j}-P_{i,j}}{\Delta X^2}\\ &-\frac{1}{2}\left\{\left(\frac{\bar{\rho}H^3}{\bar{\eta}}\right)_{i,j}+\left(\frac{\bar{\rho}H^3}{\bar{\eta}}\right)_{i-1,j}\right\}\frac{P_{i,j}-P_{i-1,j}}{\Delta X^2}\\ &+\frac{1}{2}\left\{\left(\frac{\bar{\rho}H^3}{\bar{\eta}}\right)_{i,j+1}+\left(\frac{\bar{\rho}H^3}{\bar{\eta}}\right)_{i,j}\right\}\frac{P_{i,j+1}-P_{i,j}}{\Delta Y^2}\\ &-\frac{1}{2}\left\{\left(\frac{\bar{\rho}H^3}{\bar{\eta}}\right)_{i,j}+\left(\frac{\bar{\rho}H^3}{\bar{\eta}}\right)_{i,j-1}\right\}\frac{P_{i,j}-P_{i,j-1}}{\Delta Y^2}\\ &-6U\frac{\bar{\rho}_{i+1,j}H_{i+1,j}-\bar{\rho}_{i-1,j}H_{i-1,j}}{\Delta X}\\ &-6V\left[H_{i,j}\left(\frac{\partial\bar{\rho}}{\partial P}\right)_{i,j}\frac{P_{i,j}-P^{n-1}_{i,j}}{\Delta T}+\bar{\rho}_{i,j}\frac{H_{i,j}-H^{n-1}_{i,j}}{\Delta T}\right]\end{aligned} \tag{13}$$

where, n-1 is the superscript representing a time-step that is immediately prior to the present time-step.

3.3 Analysis procedure

Figure 5 represents the procedure of the transient 3-dimensional EHL analysis for gear teeth contact. To get converged results from EHL analysis, some attention should be paid to the analysis procedure because the governing equations are non-linear and are apt to diverge accordingly. Newton-Rapson method is adopted for the analysis, as it comparatively converges well in this case. But stability of the analysis with the Newton-Rapson method is quite dependent on the initial guess. One of the remedies to obtain stability is to narrow the differences between the initial guess and the final solution. For this, 3-dimensional contact analysis is carried out first and the contact pressure distribution that satisfies the equilibrium condition of Eq. (8) is used for the initial pressure of steady EHL analysis (Koo et al., 2002). And the pressure distribution from the result of steady EHL analysis is set to the initial pressure of transient EHL analysis of the first calculation cycle. Transient EHL analysis is performed from the second calculation cycle by substituting the pressure distribution and film thickness distribution of the former time-step to the values of term with n-1 superscript in Eq. (13). Jacobian factors are calculated at each iteration and the pressure distribution that is balanced to an external load is obtained by solving the Jacobian matrix. The difference of

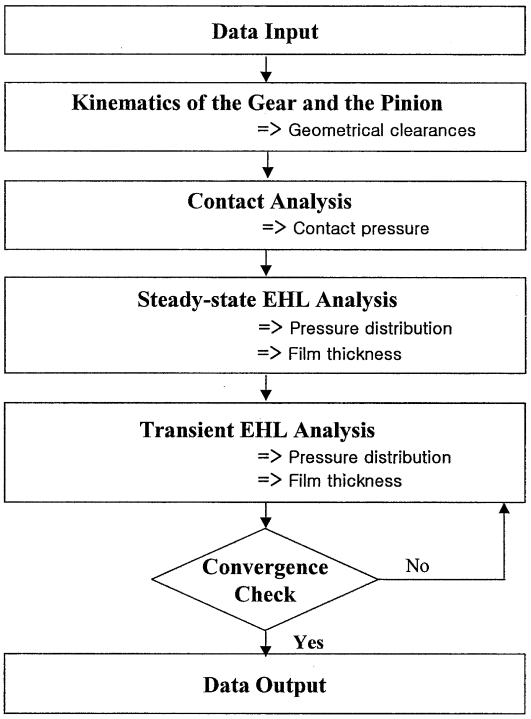

Fig. 5 Overall analysis procedure

pressures between iterations is used as convergence criterion in a time-step and the difference of film thickness between calculation cycles is used as convergence criterion in a calculation cycle as shown in Eq. (14) and Eq. (15) respectively.

$$\frac{\sum | P_{ij}^{new} - P_{ij}^{old} |}{\sum | P_{ij}^{new} |} \leq 1 \times 10^{-5} \qquad (14)$$

$$\max\left[\frac{\sum | H_{ij}^{new} - H_{ij}^{old} |}{\sum | H_{ij}^{new} |}\right] \leq 1 \times 10^{-4} \qquad (15)$$

3.4 Analysis condition

Table 1 shows the specification of the gear and the pinion and Table 2 indicates properties of the lubricant. 13 time steps are taken along the line of action for the transient analysis. Figure 6 shows both external loads and entraining velocities as a function of time steps that is the transition condition from 2 pairs of teeth in contact to 1 pair and again to 2 pairs in contact.

It is assumed that the macroscopic displacements of teeth gave no consequence on the initial film thickness because two teeth deformed the same side and the relative difference is negligible. The total film thickness is denoted by ;

$$h = h_g + h_d + h_o \qquad (16)$$

In Eq. (16), h_g is geometric clearance shape from Eq. (5) and h_d is elastic deformation of the surface due to contact pressure and h_o is a film constant. Equation (17) is introduced into an initial guess of film constant, based on the minimum film thickness formula Eq. (18) (Dowson and Higginson, 1966).

$$h_0 = 4RH_{\min} \qquad (17)$$

$$H_{\min} = 10.6 U^{0.7} G^{0.54} W^{-0.13} \qquad (18)$$

Table 1 Particulars of the gear and pinion

	Gear	Pinion
Number of teeth	24	16
Pressure angle, α	20°	
Module	4.5mm	
Face width	20.0mm	
Angular speed	1460rpm	2190rpm
Power transmitted	12kW	
Effective modulus of elasticity, E	220×10^9 N/m^2	

Table 2 Property of the lubricant

Grade	SAE30
Absolute viscosity, η_0	0.07Ns/m^2 @80℃
Pressure-viscosity coefficient, a	1.51×10^{-8}m^2/N
Dimensionless viscosity-pressure index, Z	0.4223

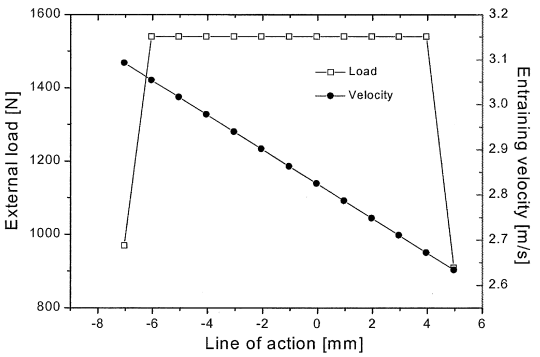

Fig. 6 External loads and entraining velocities

To relieve the peak pressure at the edges of a tooth, a profiled edge shape-radius of curvatures are getting shorter little by little to the edge-is adopted.

4. EHL Analysis Result and Discussion

Figure 7 demonstrates the pressure distribution of the contact regions between the teeth for line of action -3mm at which load is high and entraining velocity is low relatively. It indicates pressures in tooth width as well as tooth moving direction. The maximum pressure emerges on both edges of the tooth width at the outlet region. Besides the pressure spike at the outlet region, a representative phenomenon in EHL regime, the pressure at the inlet region is slightly higher than that of the center region. This phenomenon is attributable to the contact pressure pattern and contacting width of the teeth. The contact pressure between two contacting teeth in Fig. 8 shows peak values both at inlet and outlet region, which is similar to pressure distribution at contact of a punch and a

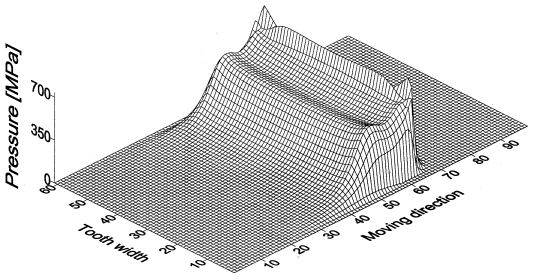

Fig. 7 EHL Pressure distribution at line of action : -3mm

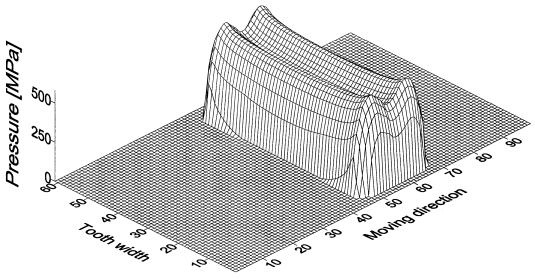

Fig. 8 Contact pressure distribution at line of action : -3mm

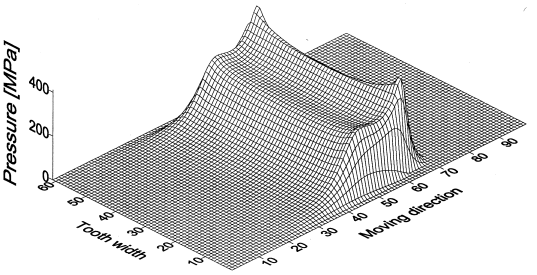

Fig. 9 EHL Pressure distribution at line of action : -7mm

plane. Namely, contact of two gear teeth is closer to narrow face contact rather than line contact. Existing 2-dimensional analysis with an assumption of two cylinders contact cannot display this phenomenon (Larsson, 1997). Figure 9 shows 3-dimensional pressure distribution for line of action -7mm at which load is low and entraining velocity is relatively high. The pressure pattern is similar to that of Fig. 7 with lower values.

Figure 10 shows pressure profiles for several time steps and Fig. 11 shows film thickness profiles at the center of tooth face respectively. Pressure profiles are similar pattern one another but pressure spikes increase with the decreasing contact width for the same load of 1540N in the range of line of action from -3mm to 4mm. Both the film profile and pressure profile are shown on Fig. 12 for the line of action 0mm. There is film constriction at outlet due to the elastic deformation of the surface and the pressure increases to peak value just before the film thickness is minimum. The pressure at contact center is lower than

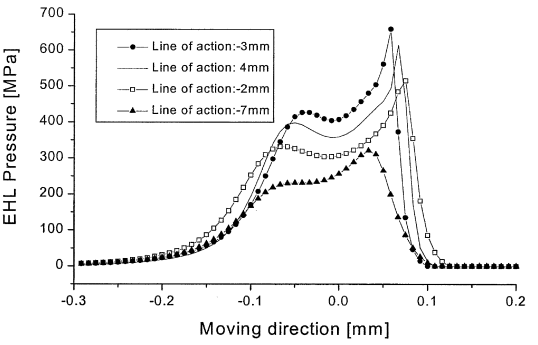

Fig. 10 EHL Pressure profiles along center plane of tooth width

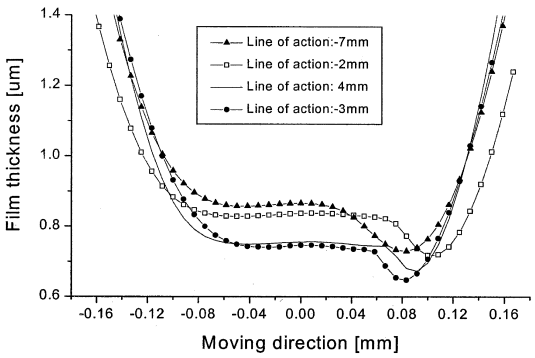

Fig. 11 Film thickness profiles along center plane of tooth width

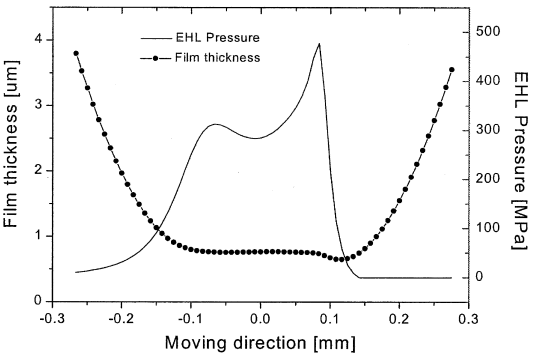

Fig. 12 EHL Pressure and film profiles at line of action : 0mm

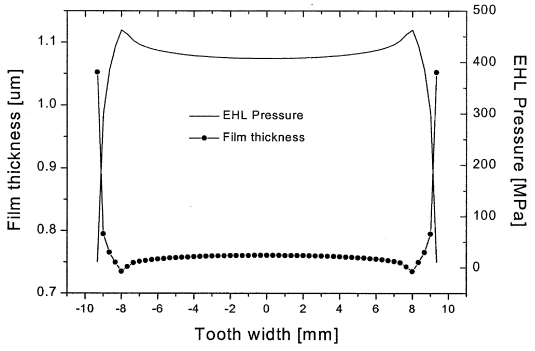

Fig. 13 EHL Pressure and film profiles along tooth width at line of action : -3mm

the one at the inlet region. Figure 13 shows both the film profile and pressure profile in face width along contact center. There are small constrictions at tooth edges and they may help to prevent side leakage of the lubricant.

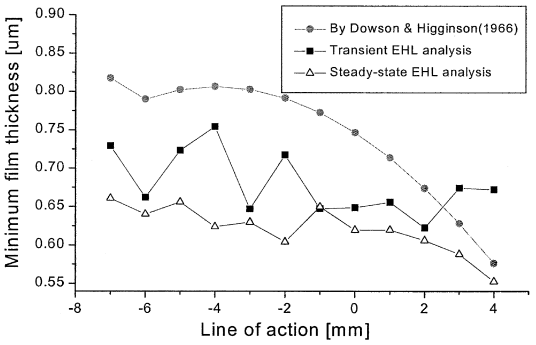

Fig. 14 Comparison of minimum film thickness

The analysis results of minimum film thickness with the assumption of steady state are compared with those of transient state. For the steady state analysis, the 2nd term of right hand side in Eq. (6) is set to null. As is shown on Fig. 14, the existence of transient term is much helpful in getting thicker film thickness. As a whole, film thickness is getting thicker with increasing velocity under the same load. Fluctuations in steady state film thickness may come from the variations of contact radius. For the transient state, film thickness is much affected by the transient term.

5. Conclusions

For a contact surface of involute spur gear teeth, the surface pressure distribution and film thickness distribution in a lubricated condition have been estimated by a transient 3-dimensional EHL analysis. Kinematics of the gear and the pinion were taken into account to obtain accurate geometric clearances around the EHL region of the contacting teeth.

The analysis results show high pressure at inlet region as well as pressure peaks at outlet region. The maximum pressures emerge at the both edges of the tooth width. Film constrictions are shown both at outlet region and teeth edges. Film thickness of transient condition is thicker than that of steady condition.

This study for the lubrication phenomenon on gear teeth could be utilized for the improvement of the gear design like modification of tooth geometry or profiling of the tooth edges.

Acknowledgments

This work was partially supported by the Brain Korea 21 Project in 2004.

References

Seol I., Chung, S., 2000, Simulation of Meshing for the Spur Gear Drive with Modified Tooth Surfaces, *KSME International Journal*, Vol. 14 No. 5, pp. 490～498.

Lee, Sang-Kwon, 1999, Application of the L-Wigner Distribution to the Diagnosis of Local Defects of Gear Tooth, *KSME International Journal*, Vol. 13 No. 2, pp. 144～157.

Jiang, Q. Y. and Barber, G. C., 1999, "Modeling of Reaction Film Failure in Gear Lubrication," *Wear*, Vol. 231, pp. 71～76.

Murakawa, M., Komori, T., Takeuchi, S., and Miyoshi, K., 1999, "Performance of a Rotating Gear Pair Coated with an Amorphous Carbon Film Under a Loss-of-Lubrication Condition," *Surface and Coatings Technology*, Vol. 120-121, pp. 646～652.

Lyu, S., Inoue, K., Deng, G., and Kato, M., 1998, Effect of Surface Treatments on the Strength of Carburized Gears An Application of Fracture Mechanics, *KSME International Journal*, Vol. 12 No. 2, pp. 206～214.

Wu, S. and Cheng, H. S., 1993, "Sliding Wear Calculation in Spur Gears," *Journal of Tribology*, Vol. 115, pp. 493～500.

Dowson, D., 1995, "Elastohydrodynamic and micro-elastohydrodynamic lubrication," *Wear*, Vol. 190, pp. 125～138.

Larsson, R., 1997, "Transient Non-Newtonian Elastohydrodynamic Lubrication Analysis of an Involute Spur gear," *Wear*, Vol. 207, pp. 67～73.

Dowson, D. and Higginson, G. R., 1966, "Elastohydrodynamic Lubrication, the Fundamentals of Roller and Gear Lubrication," Pergamon, Oxford.

Hamrock, B. J., 1994, "Fundamentals of Fluid Film Lubrication," McGRAW-HILL, pp. 141～165.

Roelands, C. J. A, 1966, Correlational Aspects of the Viscosity-Temperature-Pressure Relationship of Lubricating Oils, Doctoral thesis, Technische Hogeschool te Delt, Netherlands.

Koo, Y. P., Cho, Y. J., Lee, D. W., 2002, "3-Dimensional Elastohydrodynamic Lubrication Analysis on the Cam-Roller Contact with Consideration of Roller Profiling," *JSME International Journal*, Vol. 45(C), pp. 316～322.